OFD1 Is Mutated in X-Linked Joubert Syndrome and Interacts with *LCA5*-Encoded Lebercilin

Karlien L.M. Coene,[1,2,9] Ronald Roepman,[1,2,9,*] Dan Doherty,[4] Bushra Afroze,[5] Hester Y. Kroes,[6] Stef J.F. Letteboer,[1] Lock H. Ngu,[5] Bartlomiej Budny,[7] Erwin van Wijk,[3] Nicholas T. Gorden,[4] Malika Azhimi,[1] Christel Thauvin-Robinet,[8] Joris A. Veltman,[1,2] Mireille Boink,[1] Tjitske Kleefstra,[1] Frans P.M. Cremers,[1,2] Hans van Bokhoven,[1,2] and Arjan P.M. de Brouwer[1,2]

We ascertained a multi-generation Malaysian family with Joubert syndrome (JS). The presence of asymptomatic obligate carrier females suggested an X-linked recessive inheritance pattern. Affected males presented with mental retardation accompanied by postaxial polydactyly and retinitis pigmentosa. Brain MRIs showed the presence of a "molar tooth sign," which classifies this syndrome as classic JS with retinal involvement. Linkage analysis showed linkage to Xpter-Xp22.2 and a maximum LOD score of 2.06 for marker DXS8022. Mutation analysis revealed a frameshift mutation, p.K948NfsX8, in exon 21 of *OFD1*. In an isolated male with JS, a second frameshift mutation, p.E923KfsX3, in the same exon was identified. *OFD1* has previously been associated with oral-facial-digital type 1 (OFD1) syndrome, a male-lethal X-linked dominant condition, and with X-linked recessive Simpson-Golabi-Behmel syndrome type 2 (SGBS2). In a yeast two-hybrid screen of a retinal cDNA library, we identified OFD1 as an interacting partner of the *LCA5*-encoded ciliary protein lebercilin. We show that X-linked recessive mutations in *OFD1* reduce, but do not eliminate, the interaction with lebercilin, whereas X-linked dominant *OFD1* mutations completely abolish binding to lebercilin. In addition, recessive mutations in *OFD1* did not affect the pericentriolar localization of the recombinant protein in hTERT-RPE1 cells, whereas this localization was lost for dominant mutations. These findings offer a molecular explanation for the phenotypic spectrum observed for *OFD1* mutations; this spectrum now includes OFD1 syndrome, SGBS2, and JS.

Introduction

Joubert syndrome (JS [MIM 213300]) is characterized by a specific mid-hindbrain malformation, hypotonia, cerebellar ataxia, and developmental delay. Oculomotor apraxia and abnormalities in breathing patterns are frequently part of this condition as well. The typical cerebellar and brainstem malformations in JS result in a characteristic neuroradiological hallmark known as the "molar tooth sign."[1] The molar tooth sign is not restricted to classical JS but has also been observed in disorders in which more organ systems are affected. This group of syndromes was termed Joubert syndrome and related disorders (JSRDs)[2], and a classification into six subgroups has been proposed.[3] Apart from the classical form, JS can occur in combination with progressive retinal degeneration,[4] renal abnormalities (nephronophthisis, NPHP [MIM 256100]),[5] both retinal and renal involvement (cerebello-oculo-renal syndromes, CORS [MIM 608091]),[6] ocular colobomas and liver abnormalities (COACH [MIM 216360]),[7] and both orofacial and digital signs (OFDVI [MIM 277170]).[8] These additional features are characteristic of disorders caused by primary cilium and/or basal-body dysfunction,[9] indicating that the pathogenic mechanism in JSRDs probably involves defective cilium and/or basal-body function.

So far, nine autosomal JSRD loci have been mapped, and causative genes have been identified for eight of these.[3,10] All eight JSRD genes encode proteins that localize to cilia or centrosomes, reiterating ciliary dysfunction as a key factor in the molecular pathogenesis of JSRDs. The *AHI1* (MIM 608894) gene is most frequently associated with a combination of JS and retinopathy and encodes jouberin, which physically interacts with the *NPHP1*-encoded nephrocystin-1 protein (MIM 607100).[11–13] *ARL13B* (MIM 608922) encodes a small GTPase that belongs to the Arf/Arl class of the Ras GTPase family.[10] Animal *ARL13B*-null models emphasize the ciliary importance of this gene in that they reproduce cilia-related phenotypes such as disruption of neural-tube development, renal cysts, and overall defective cilium morphology.[14,15] The protein product encoded by the *CC2D2A* (MIM 612013) gene functions in close association with the centrosomal protein CEP290.[16] A nonsense mutation in the zebrafish *CC2D2A* ortholog (*sentinel*) results in the formation of pronephric cysts.[16] The most recently identified JSRD gene is *INPP5E*, which is the causative gene for the *JBTS1* locus. The encoded protein functions in phosphatidyl inositol signaling, linking this pathway to the ciliopathies.[17] The remaining four JSRD genes have also been implicated in other overlapping human ciliary disorders: *NPHP1* in isolated NPHP,[18]

[1]Department of Human Genetics, [2]Nijmegen Center for Molecular Life Sciences, [3]Department of Otorhinolaryngology, Radboud University Nijmegen Medical Centre, Nijmegen 6500 HB, The Netherlands; [4]Department of Pediatrics, University of Washington School of Medicine and Seattle Children's Hospital, Seattle, WA 98195, USA; [5]Division of Clinical Genetics, Pediatrics Institute, Kuala Lumpur Hospital, Kuala Lumpur 50586, Malaysia; [6]Department of Medical Genetics, University Medical Center Utrecht, Utrecht 3508 AB, The Netherlands; [7]Department of Medical Genetics, Poznan University of Medical Sciences, Poznan 60-352, Poland; [8]Centre de Génétique, Hôpital d'Enfants, Dijon 21079, France
[9]These authors contributed equally to this work.
*Correspondence: r.roepman@antrg.umcn.nl
DOI 10.1016/j.ajhg.2009.09.002.

TMEM67/MKS3[19] (MIM 609884), *RPGRIP1L*[20,21] (MIM 610937), and also *CC2D2A*[22] in Meckel syndrome (MIM 249000), and *CEP290* (MIM 610142) in isolated Leber congenital amaurosis (LCA [MIM 204000]),[23] Senior-Løken syndrome (SLS, a combination of retinal degeneration and NPHP [MIM 266900]),[24] and Meckel syndrome.[25] The exact biochemical pathway in which JSRD proteins play a role remains unclear. However, experimental evidence is pointing to cilia-mediated Sonic hedgehog (Shh) signaling as a likely candidate.[15,20,26]

In this study, we have identified mutations in exon 21 of the *OFD1* (MIM 311200) gene in two families with classical JS, thereby defining *OFD1* as the JBTS10 locus. In one family, patients also suffer from retinal pathology. To our knowledge, this is the first report of X-linked inheritance in JS and of mutations in *OFD1* downstream of exon 17. The *OFD1* gene has previously been associated with oral-facial-digital type 1 (OFD1) syndrome (MIM 311200),[27] which is a male-lethal X-linked dominant condition involving malformations of the face, oral cavity, and digits in affected females. Budny and coworkers also described a single family in which *OFD1* was found to be mutated in Simpson-Golabi-Behmel syndrome type 2 (SGBS2 [MIM 300209]).[28] We show that OFD1 directly binds to the ciliary protein lebercilin, encoded by the *LCA5* (MIM 611408) gene.[29] Mutations in *LCA5* cause LCA, an inherited condition of very early-onset childhood blindness that is due to retinal degeneration and also belongs to the ciliopathy spectrum. We also show that X-linked recessive mutations in *OFD1* reduce, but do not eliminate, the interaction with lebercilin and do not affect ciliary localization in cell lines, whereas X-linked dominant *OFD1* mutations completely abolish binding with lebercilin and disrupt ciliary localization as well. Our findings offer a molecular explanation for the phenotypic variability observed in *OFD1*-related disorders.

Material and Methods

Patients

In all patients from family W07-713, karyotypes at a resolution of 550 bands were normal, and expansions of the CGG repeat in the 5′-untranslated region of *FMR1* were excluded. In patient IV-10, submicroscopic copy-number variations larger than 100 kb were excluded by Affymetrix 250k SNP array analysis in which was used as a restriction enzyme according to the manufacturer's protocols (Affymetrix, Santa Clara, CA, USA). Copy-number estimates were made with the CNAG software package v. 2.0.[30] In addition, probands from 84 JS families in which only males were affected were selected from a cohort of 250 families. All families showed a molar tooth sign on MRI scan and had developmental delay and ataxia. Known genes and loci for JSRD (*AHI1*, *ARL13B*, *CC2D2A*, *CEP290*, *NPHP1*, *RPGRIP1L*, *TMEM67*, and chromosomal loci 9q34 and 11p11.2–q12.1) were excluded in most cases by direct sequencing or segregation analysis. All DNA samples were isolated from whole blood by the salting-out method as described by Miller et al.[31] Informed consent was obtained for all patients, and research was approved by the respective local ethics committees.

X-Chromosomal Linkage Analysis

Polymorphic short-tandem-repeat markers on the X chromosome were selected with an average distance of 10 cM between the markers. Primers for amplifying these markers were designed with the Primer3 program.[32] An M13 tail was added to the 5′ and 3′ ends of the primers. Markers were amplified with an M13 forward primer labeled with one of the fluorophores, FAM, VIC, NED, or ROX, at the 5′ end[33] and an M13 reverse primer with a 5′-GTTTCTT-3′ added to its 5′ end so that tailing would be reduced.[34] Primer sequences are given in Table S1. PCR conditions are available on request. Final PCR products were mixed with eight volumes of formamide and half a volume of Genescan 500(−250) LIZ size standard (Applied Biosystems, Foster City, CA, USA) and analyzed with the ABI PRISM 3730 DNA analyzer (Applied Biosystems). The results were evaluated by Genemapper (Applied Biosystems). Two-point LOD scores were calculated by Superlink[35], and exclusion mapping was performed with GeneHunter PLUS v. 1.2[36]; both programs are integrated in the computer program easyLINKAGE.[37] Inheritance model was set at recessive, and the frequency of the disease allele was set at 0.001. Full penetrance was assumed.

DNA Sequencing

Primers for amplification of all exons of *OFD1* (GenBank ID NM_003588.3) were designed with the Primer3 program (Table S1).[32] Of the last exon, 374 nucleotides of the 3′-untranslated region were analyzed. PCR conditions are available on request. The ABI PRISM BigDye Terminator Cycle Sequencing v. 2.0 Ready Reaction Kit was used for sequencing PCR products with the same forward and reverse primers as those used in the PCR, and the products were analyzed with the ABI PRISM 3730 DNA analyzer (Applied Biosystems).

Amplification Refractory Mutation System

Amplification Refractory Mutation System (ARMS) primers for specific amplification of either the wild-type or mutant allele were designed with the Primer3 program (Table S1).[32] The wild-type or mutant alleles were amplified from 50 ng DNA by the use of 10 U *Taq* polymerase (Invitrogen, Breda, The Netherlands) in *Taq* buffer, 2.0 mM $MgCl_2$, 0.25 mM dNTPs (Invitrogen, Breda, The Netherlands), and 100 nM forward and reverse primers in a total volume of 25 μl. PCR cycling conditions consisted of (1) denaturation at 95°C for 10 min, (2) 40 cycles of amplification by denaturation at 95°C for 15 s, annealing at 58°C for 15 s, and elongation at 72°C for 15 s, and (3) final elongation at 72°C for 10 min. PCR products were analyzed on a 1.5% agarose gel.

X Inactivation

Skewing of X inactivation was investigated via analysis of the CGG repeat in the promoter region of *FMR1*, for which the tested carrier females had two different alleles. One microgram DNA from carrier females and a male control was digested overnight at 37°C with a combination of 40 U BamHI (Westburg, Leusden, The Netherlands) and 20 U of the methylation-sensitive restriction enzyme HhaI (Westburg), as well as 40 U BamHI alone as a control, in NEB buffer 4 (Westburg) in a total volume of 50 μl. Subsequently, complete digestion was ensured by redigestion of the DNA for 4 hr at 37°C via addition of half of the units of BamHI and HhaI initially used in the reaction mixtures. The enzymes were heat inactivated at 65°C for 20 min. The CGG repeat was amplified from 2.5 μl digestion mixture by 3 U *Taq* polymerase

(Invitrogen, Breda, The Netherlands) in Pfx Amp buffer (Invitrogen, Breda, The Netherlands), 1.5 mM $MgSO_4$, 0.25 mM dNTPs (Invitrogen, Breda, The Netherlands), 4× PCR enhancer solution (Invitrogen, Breda, The Netherlands), and 300 nM forward and 5′-FAM-labeled reverse primers (Table S1) in a total volume of 20 μl. PCR cycling conditions consisted of (1) denaturation at 95°C for 10 min, (2) 32 cycles of amplification by denaturation at 95°C for 15 s, annealing at 64°C for 2 min, and elongation at 75°C for 2 min, and (3) final elongation at 72°C for 10 min. PCR products were analyzed as described in the X-Chromosomal Linkage Analysis section. Complete digestion of one of the two alleles was confirmed by the absence of a PCR product in the BamHI- and HhaI-digested DNA of the hemizygous male control, whereas in all other samples at least one allele was amplified.

Cell Culturing

Human B-lymphocytes were immortalized by transformation with Epstein-Barr virus according to established procedures.[38] EBV-LCLs from patients and controls were grown at 37°C and 7.5% CO_2 in RPMI 1640 medium (GIBCO, Breda, The Netherlands) containing 10% (v/v) fetal calf serum (Sigma, Zwijndrecht, The Netherlands), 1% 10 U/μl penicillin and 10 μg/μl streptomycin (GIBCO), and 1% GlutaMAX (GIBCO). Twenty-four hours before emetin treatment, cells were centrifuged at 200 × *g* for 5 min at room temperature and resuspended in fresh medium to a density of 0.7 million cells per ml. Cells were treated with 100 μg/ml emetin for 10 hr. Subsequently, 5–10 million cells were harvested by centrifugation at 200 × *g* for 5 min at room temperature, washed with PBS, and pelleted by centrifugation at 200 × *g* for 5 min at room temperature. Pellets for RNA isolation were snap frozen in liquid nitrogen.

RNA Isolation and First-Strand Synthesis

Total RNA was isolated with the NucleoSpin RNA II kit (Macherey-Nagel, Düren, Germany) according to the manufacturer's protocol. For removing residual traces of genomic DNA, the RNA was treated with DNase I (Invitrogen, Leek, The Netherlands) while bound to the RNA-binding column. The integrity of the RNA was assessed on 1.2% agarose gel, and the concentration and purity were determined by optical densitometry. One microgram of total RNA was transcribed into cDNA with the iScript cDNA synthesis kit (Bio-Rad Laboratories, Hercules, CA, USA) according to the manufacturer's protocol. cDNA was purified with the NucleoSpin extract II kit (Macherey-Nagel) according to the manufacturer's protocol.

Quantitative PCR

SYBR Green-based real-time quantitative PCR (QPCR) analysis was performed on a 7500 Fast Real-Time PCR System (Applied Biosystems) with Power SYBR Green PCR Master Mix (Applied Biosystems) according to the manufacturer's instructions. Primers were developed by the Primer3 program[32] (Table S1) and validated as described before.[39] PCR products encompassed at least one exon-exon junction. *GUSB* was used as reference gene. QPCR quantifications were performed in duplicate on the equivalent of 400 pg/μl input of total RNA in the first-strand synthesis and included a reverse-transcriptase control. Values for experimental threshold cycles (Ct) were within the range of cDNA dilutions used for validating the primers. The melt curves of all PCR products showed a single PCR product. All controls were negative. Differences in the expression of a gene of interest between two samples were calculated by the comparative Ct or $2^{\Delta\Delta Ct}$ method.[40,41]

DNA Constructs

Constructs encoding the full-length OFD1 variant of 1012 amino acids ($OFD1^{FL}$; NCBI Reference Sequence: NM_003611.2 [gene]; NP_003602.1 [protein]) were generated by PCR with an *OFD1* cDNA clone that was kindly donated by Prof. Brunella Franco (TIGEM Telethon Institute of Genetics and Medicine, Naples, Italy). For this variant, the Coils2 program[42] predicts six coiled-coil domains. For the constructs encoding coiled-coil domains two/three (fusion of coiled-coil domains two and three) and four and coiled-coil domains five and six of OFD1, *OFD1* cDNA IMAGE clone (GenBank BC096344) (imaGenes, Berlin, Germany) was used as a template in PCR. This clone contains an alternative splice variant that lacks exon 10 and thus encodes a 972 amino acid variant protein ($OFD1^{\Delta ex10}$) that lacks the corresponding amino acids 313–353. For this splice variant, five coiled-coil domains are predicted because coiled-coil domains two and three are fused into one larger coiled-coil domain (coiled-coil domain two/three). The OFD1 constructs encoding amino acids 240–1012 and amino acids 356–1012 were generated by PCR on template DNA from the corresponding clones that were identified in the yeast two-hybrid assay, from which the first clone includes exon 10. Expression constructs were created with Gateway technology (Invitrogen, Leek, The Netherlands) according to the manufacturer's instructions. *LCA5* constructs were generated as previously described.[29] Constructs for OFD1 mutants were generated by site-directed mutagenesis PCR. Primers are available upon request. The sequence of all entry clones was verified by nucleotide sequencing.

Yeast Two-Hybrid Assays

The GAL4-based yeast two-hybrid system (HybriZAP, Stratagene, La Jolla, USA) was used for identifying protein-interaction partners of lebercilin. The region encompassing the first 305 N-terminal amino acids of lebercilin, fused to a DNA-binding domain (GAL4-BD), was used as a bait for sreening a human oligo-dT primed retinal cDNA library. The yeast strain *PJ69-4A*, which carried the *HIS3* (histidine), *ADE2* (adenine), *MEL1* (α-galactosidase) and *LacZ* (β-galactosidase) reporter genes, was used as a host. Interactions were analyzed by assessment of reporter gene activation via growth on selective media (*HIS3* and *ADE2* reporter genes), α-galactosidase colorimetric plate assays (*MEL1* reporter gene), and β-galactosidase colorimetric filter lift assays (*LacZ* reporter gene). For analysis of the binding capacities of OFD1 mutant proteins to lebercilin, expression constructs encoding amino acids 356–1012 of OFD1 as a GAL4-AD-fusion protein, either wild-type or containing the p.K948fs, p.K923fs, p.I784fs, p.E709fs, p.N630fs, or p.S586fs mutation, were cotransformed with a construct encoding the first two coiled-coil domains of lebercilin fused to GAL4-BD (pBD-$lebercilin^{CC1+2}$) in *PJ69-4α*. As a negative control, the empty pAD vector was cotransformed with pBD-$lebercilin^{CC1+2}$. Protein interactions were evaluated on the basis of growth on selective media and staining in α- and β-galactosidase activity assays. The interactions of wild-type and mutant OFD1 with wild-type lebercilin were semi-quantified with a liquid β-galactosidase assay. Liquid cultures of *PJ69-4α*, cotransformed with combinations of pAD-OFD1 and pBD-lebercilin ($n = 4$ for each combination), were grown for 24 hr at 30°C in SD medium lacking leucine and tryptophan. Subsequently, the optical density of the cultures was determined at a wavelength

of 600 nm for data normalization. Cell lysis and colorimetric reactions were performed with the Yeast β-galactosidase assay kit (Pierce Biotechnology, Rockford, IL, USA) according to the manufacturer's instructions. β-galactosidase activity was determined from absorbance at a wavelength of 420 nm. For the calculation of relative remaining reporter gene activity, values were corrected for background activity in the assay.

Colocalization in hTERT-RPE1 Cells

hTERT-RPE1 cells (kindly provided by Prof. Uwe Wolfrum, Johannes-Gutenberg Universität, Mainz, Germany) were cultured as previously described.[16] This is a human retinal pigment epithelial (RPE) cell line that is immortalized by stable expression of human telomerase reverse transcriptase (hTERT) (Clontech, Saint-Germain-en-Laye, France). Cells were seeded on coverslips and were serum starved for 24 hr prior to transfection so that primary cilium formation would be induced. Subsequently, Effectene (QIAGEN, Venlo, The Netherlands) was used for transfecting cells. Single constructs encoding either wild-type or mutant OFD1 fused to enhanced cyan fluorescent protein (eCFP) or a combination of constructs encoding eCFP-OFD1 and constructs encoding full-length lebercilin fused to monomeric red fluorescent protein (mRFP) were transfected. After 24 hr, cells were fixed in icecold methanol for 10 min, treated with 1% Triton X-100 in phosphate-buffered saline (PBS) for 5 min, and blocked in 2% bovine serum albumine in PBS for 20 min. Incubation with the primary antibody GT335 (mouse monoclonal antibody, kindly provided by Carsten Janke, CNRS Centre de Recherches en Biochimie Macromoléculaire, Montpellier, France) was performed for 1 hr. After being washed in PBS, coverslips were stained with goat-anti-mouse Alexa 568 (Invitrogen, Leek, The Netherlands) for 45 min. Coverslips were washed again with PBS and briefly with mQ before being mounted in Vectashield containing DAPI (Vector Laboratories, Burlingame, CA, USA). The localization of constructs was analyzed with a Zeiss Axio Imager Z1 fluorescence microscope equipped with a 63× objective lens.

GST Pull-Down Assay

Both OFD1 splice variants and OFD1 fragments (amino acids 240–1012 and amino acids 356–1012) were cloned into pDEST15 (Gateway cloning system, Invitrogen, Karlsruhe, Germany). For the creation of GST-fusion proteins, BL21-DE3 cells were transformed with pDEST15 constructs. Cells were induced overnight with 0.5 mM IPTG at 30°C and subsequently lysed in STE buffer (10 mM Tris-HCl [pH 8.0], 1 mM EDTA, and 150 mM NaCl) supplemented with 10 mg/ml Lysozyme, 0.5% Sarkosyl, 1% Triton X-100, and complete protease inhibitor cocktail (Roche Diagnostics, Mannheim, Germany). Lysates were incubated with glutathione-sepharose 4B beads (Amersham Biosciences, Freiburg, Germany). After incubation, beads were washed with STE and TBSTD (TBS with 1% Triton X-100 and 2 mM DTT). The amount of GST-fusion proteins bound to the beads was verified on a NuPAGE Novex 4%–12% Bis-Tris SDS–PAGE gel by staining with SimplyBlue SafeStain (Invitrogen, Leek, The Netherlands). Beads with bound GST-fusion proteins were incubated for 2.5 hr at 4°C with lysates of COS-1 cells expressing 3xFLAG-tagged full-length human lebercilin. After incubation, beads with bound protein complexes were washed in lysis buffer, and this was followed by a washing step with Complex Washing Buffer (50 mM Tris-HCl [pH 7.5], 100 mM NaCl, 2 mM $MgCl_2$, 2 mM $CaCl_2$, 1% TritonX-100, and 2 mM DTT). Then beads were taken up in 4× NuPage Sample Buffer and heated for 10 min at 70°C. Beads were precipitated by centrifugation, and supernatant was loaded on a NuPAGE Novex 4%–12% Bis-Tris SDS–PAGE gel. The presence of 3xFLAG-lebercilin in complex with GST-OFD1 was assessed by immunoblotting, followed by staining with a monoclonal mouse α-FLAG primary antibody (Sigma-Aldrich, Zwijndrecht, The Netherlands) and goat-anti mouse coupled to IRDye800 (Rockland Immunochemicals, Gilbertsville, PA, USA) as a secondary antibody. Fluorescence was analyzed on a Li-Cor Odyssey 2.1 infrared scanner.

Coimmunoprecipitation

HA-lebercilin (full-length) and 3xFLAG-OFD1 (both splice variants and fragments encompassing amino acids 240–1012 and amino acids 356–1012) were coexpressed in HEK293T cells. As a negative control, HA-lebercilin was coexpressed with the functionally unrelated 3xFLAG-LRRK2 (Leucine-Rich Repeat Kinase2) protein. As a positive control, the previously described interaction between nephrocystin4 and RPGRIP1 was used.[43] After 48 hr of expression, cells were lysed on ice in lysis buffer (50 mM Tris–HCL [pH 7.5], 150 mM NaCl, 0.5% Triton X-100) supplemented with complete protease inhibitor cocktail. Lysates were incubated with anti-HA affinity matrix (Roche, Woerden, The Netherlands), or with anti-FLAG M2-agarose from mouse (Sigma-Aldrich, Zwijndrecht, The Netherlands), for 5 hr at 4°C. After incubation, beads with bound protein complexes were washed in lysis buffer. Then beads were taken up in 4× NuPage Sample Buffer and heated for 10 min at 70°C. Beads were precipitated by centrifugation, and supernatant was run on a NuPAGE Novex 4%–12% Bis-Tris SDS-PAGE gel. The interaction of 3xFLAG-OFD1 with HA-lebercilin was assessed by immunoblotting, followed by staining with either monoclonal mouse α-FLAG or monoclonal mouse α-HA (Sigma-Aldrich, Zwijndrecht, The Netherlands) as a primary antibody and goat-anti mouse RDye800 as a secondary antibody. Fluorescence was analyzed on a Li-Cor Odyssey 2.1 infrared scanner.

Immunofluorescence Labeling of Rat Retinas

Unfixed eyes of 20-day-old (p20) Wistar rats were harvested and frozen in melting isopentane. Seven micrometer cryosections were cut and treated with 0.01% Tween in PBS and subsequently blocked in blocking buffer (0.1% ovalbumin and 0.5% fish gelatin in PBS). Then the cryosections were incubated overnight with primary antibodies diluted in blocking buffer, either with affinity-purified α-lebercilin rabbit serum[29] in combination with a mouse α-centrin monoclonal antibody (kindly provided by Prof. Uwe Wolfrum, Johannes-Gutenberg Universität, Mainz, Germany) or with affinity-purified α-OFD1 rabbit serum (kindly provided by Prof. E. Nigg, Max-Planck Institut für Biochemie, Martinsried, Germany) in combination with a mouse α-centrin monoclonal antibody. Secondary antibodies were also diluted in blocking buffer and incubated in a dark environment for 1 hr. Prolong Gold Antifade (Molecular Probes, Leiden, The Netherlands) was used for embedding the sections. Pictures were made with an Axioskop2 Mot plus fluorescence microscope (Zeiss, Oberkochen, Germany), which was equipped with an AxioCam MRC5 camera (Zeiss). Images were processed with Axiovision 4.3 (Zeiss) and Adobe Photoshop (Adobe Systems, San Jose, CA, USA). Procedures were in accordance with the ethical standards of the responsible committee on animal experimentation.

Expression Analysis of OFD1 Isoforms

Total RNA from different human tissues was ordered from Stratagene (La Jolla, CA, USA) except for retina total RNA, which was

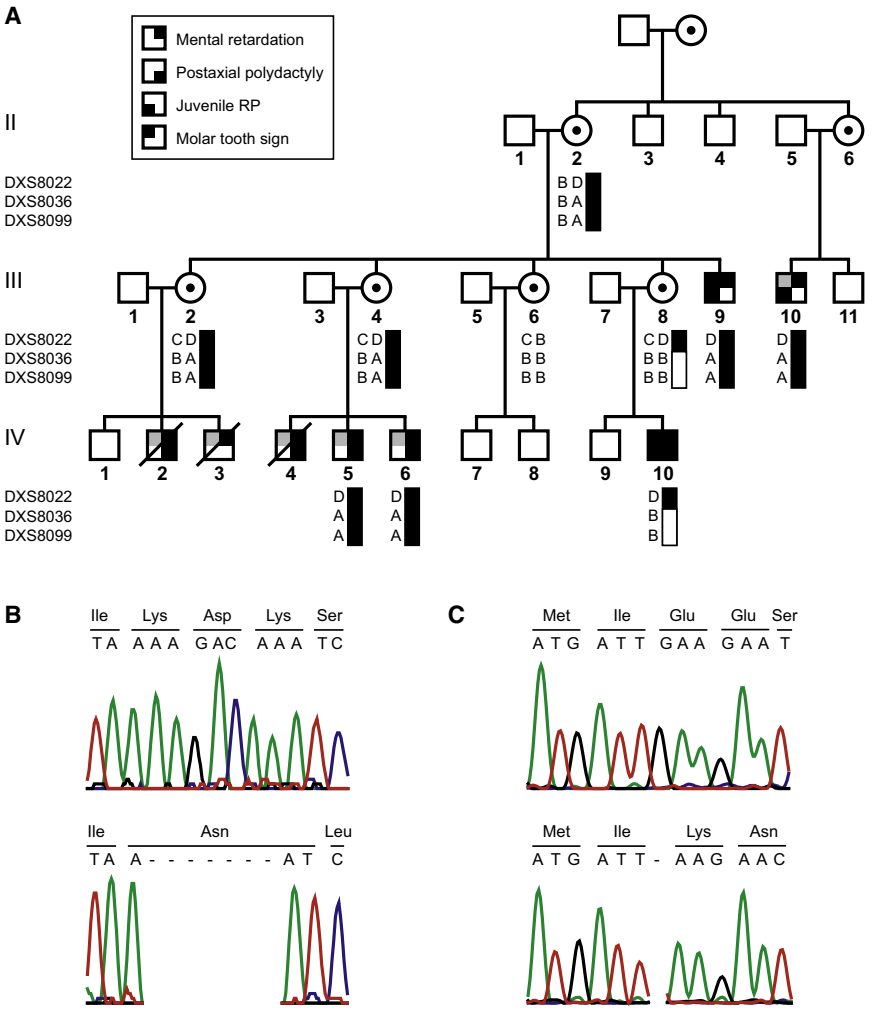

Figure 1. Pedigree and Mutation Analysis of Family W07-713

(A) Pedigree of family W07-713. Indicated are the four discerning clinical features of the patients in the family: mental retardation, postaxial polydactyly, juvenile RP, and the presence of a molar tooth sign on an MRI scan. Indicated in gray are the patients who were not investigated by MRI.

(B) Chromatograms showing the wild-type sequence in family member III-7 (up) and the c.2841_2847 delAAAAGAC deletion in patient IV-10 (down) in exon 21 of *OFD1*.

(C) Chromatograms showing the wild-type sequence in the healthy father (up) and the c.2767 delG mutation in patient UW87 (down) in exon 21 of *OFD1*.

purchased from Clontech (Saint-Germain-en-Laye, France). cDNA synthesis was performed as described above. PCR primers positioned on exon 8 and on the boundary of exons 13 and 14 are given in Table S1. PCR was stopped at cycles 25, 30, and 35. Specific PCR conditions are available on request. So that OFD1 protein isoform expression in bovine retina could be investigated, retinal extracts were made from fresh bovine retinas, obtained from the local slaughterhouse. Retinas were lysed by sonification for 1 min in lysisbuffer (50 mM Tris-HCl [pH 7.4], 150 mM NaCl, 0,5% Nonidet-P40, and 1 mM Natrium-orthovanadate) supplemented with protease inhibitors (Roche Diagnostics, Mannheim, Germany). Retinal extract was run on a NuPAGE Novex 4%–12% Bis-Tris SDS–PAGE gel. OFD1 protein expression was analyzed by immunoblotting, followed by staining with rabbit α-OFD1 polyclonal antibody and goat-anti mouse RDye800 (Rockland Immunochemicals, Gilbertsville, PA, USA) as a secondary antibody. Fluorescence was analyzed on a Li-Cor Odyssey 2.1 infrared scanner.

Results

Clinical Descriptions

Family W07-713 consists of eight males with severe to profound mental retardation (Figure 1A). Family members IV-5, IV-6, and IV-10 also have postaxial polydactyly in all four limbs. The deceased males IV-2 and IV-4 shared this feature. Retinitis pigmentosa (RP) was noticed in family members III-9, III-10, and IV-10. All patients had recurrent infections, of which family members IV-2, IV-3, and IV-4 died. None of the patients were obese, and all had normal genitalia. No abnormalities were noticed by renal ultrasound scanning. None of the female family members had any symptoms similar to those of the male patients, indicating that the inheritance pattern is most likely X-linked recessive.

Patients IV-10 and III-9 were investigated in more detail. Patient IV-10 was born at term by a lower-segment cesarean section. His birth weight was 3050 g (50th percentile), his length was 48.5 cm (25th percentile), and his head circumference was 34.5 cm (25th percentile). Soon after birth, he presented with stridor and intermittent cyanosis and was thought to have central apnea. He also had feeding problems that required tube feeding. A delay in his development was apparent: he was not able to sit or stand at the age of 3.5 years, although he could roll over at 6 months of age. All growth parameters were below −2 standard deviations (SD). The patient had apparent postaxial polydactyly of all four limbs, although central polydactyly could not be excluded (Figure 2B). He presented with mild hirsutism, had low-set ears, a broad nasal bridge, prominent philtrum and maxillary arch, and full lips (Figure 2A). Fingers and nails were normal, as were his genitalia. He could not speak, was unable to grasp or reach out for objects, and responded minimally to eye contact or sounds. He was easily irritated and had frequent temper tantrums during which he bit his tongue and lips. In addition, every two weeks he had unexplained fevers that could be treated by antipyretics. There were no serious infections that required hospital admission. The patient

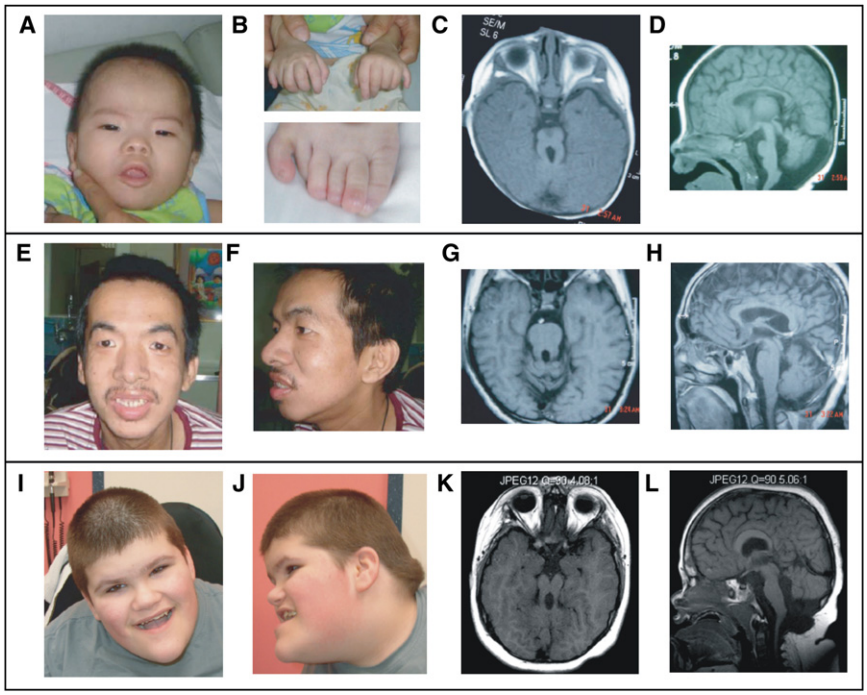

Figure 2. Clinical Phenotype of Family W07-713 and Isolated Patient UW87

(A–D) Shown are photographs of (A) the face and (B) hands and foot, as well as (C and D) brain MRI images, of patient IV-10 at the age of 1 year. Note the low-set ears, broad nasal bridge, prominent philtrum and maxillary arch, full lips, and postaxial polydactyly of all four limbs, although central polydactyly can not be excluded. On an axial T1-weighted brain MRI, a clear molar tooth sign is visible.

(E–H) Shown for patient III-9, who was 34 yrs-old at the time of examination, are (E) frontal and (F) side views of the face and (G and H) brain MRI images. This patient also has low-set ears, a broad nasal bridge, a prominent philtrum and maxillary arch, and full lips. No polydactyly was present. An axial T1-weighted MRI image showed a molar tooth sign.

(I–L) For patient UW87, who was examined at the age of 12 yrs, (I) frontal and (J) side views of the face, as well as (K and L) axial T1-weighted brain MRI images, are shown. This patient showed macrocephaly and obesity. Polydactyly was reported, but the sixth finger was removed shortly after birth. A molar tooth sign was evident from MRI images.

had retinal degeneration pointing to juvenile RP. He also had conductive hearing impairment that might be explained by the bilateral middle-ear effusion. Routine blood analysis showed no aberrations in hematologic values, liver function, or renal function; a renal sonography and echocardiogram were also normal. A brain MRI showed a molar tooth sign, hypoplasia of the cerebellar vermis, thickening of the superior cerebellar peduncles, and deep interpeduncular fossa (Figure 2C). Furthermore, patient IV-10 had a small pons and prominent medulla (Figure 2D).

Patient III-9 had severe mental retardation and was unable to care for himself. Breathing problems in early childhood were not noticed. He had low-set ears, a broad nasal bridge, a prominent philtrum and maxillary arch, and full lips, but no postaxial polydactyly (Figures 2E and 2F). He had recurrent respiratory infections during early childhood. By the age of 34, his vision was deteriorated to such an extent that he could only see shadows. Renal sonography showed no aberrations, but from the age of 31 onward, he had hypertension. An MRI scan of the brain also showed a molar tooth sign (Figure 2G), although it was more subtle than that of patient IV-10. Hypoplasia of the cerebellar vermis and thick superior cerebellar peduncles, as well as a cavum velum interpositum and mild volume loss in the cerebral and cerebellar hemispheres, were seen on a brain MRI, suggesting atrophy. The pons and medulla appeared normal in this patient (Figure 2H).

Patient UW87 is part of a cohort of 84 male JS patients who were screened for mutations after the identification of *OFD1* as a JS gene. He was born to healthy nonconsanguineous parents at 41 weeks gestation by cesarean section for failure to progress, after a pregnancy complicated by polyhydramnios. His birth weight was 4090 g, his length was 53 cm (90^{th} percentile), and his head circumference was 35.5 cm (50^{th} percentile). As a newborn, he was noted to have tongue thrusting, distinctive craniofacial features, and postaxial polydactyly of both hands and the left foot. Brain MRIs performed at 3 weeks and 8 years of age demonstrated a molar tooth sign (Figure 2K), a small occipital encephalocele, and shortening of the corpus callosum (Figure 2L). A history of repeated middle-ear infections in early childhood required pressure equalization tubes, but no serious infections were reported. A gastrostomy tube was required because of feeding difficulties. On evaluation at 12 years of age, severe intellectual disability, ambulation difficulties, and hyperphagia with obesity were noted. He used a wheelchair and walker for mobility, lacked discernable words, and was not toilet trained. On examination, he had macrocephaly (head circumference 58.1 cm, $>97^{th}$ percentile) and generalized obesity (97.7 kg, $>97^{th}$ percentile), and his height could not be measured because of combativeness and stooping (Figures 2I and 2J). He had deep-set eyes, narrowed palpebral fissures, a left-sided preauricular pit, a flattened midface, a midline upper-lip notch, a deep midline groove of the tongue, a prominent jaw, and redundant neck tissue. His extremities were notable for relative brachydactyly, fetal finger pads, small feet (US size 5 shoes), and lateral deviation and contractures at the knees. He had normal male genitalia and Tanner stage 3-4 pubic hair. On neurological examination,

Table 1. Two-Point LOD Scores for 16 X-Chromosomal Markers

Marker	Position (cM)	$\theta = 0$	$\theta = 0.05$	$\theta = 0.1$	$\theta = 0.15$	$\theta = 0.2$
DXS8022	27.46	2.07*	1.88	1.68	1.47	1.25
DXS8036	30.31	−5.63	0.34	0.49	0.51	0.47
DXS8099	42.25	−5.65	0.33	0.48	0.50	0.46
DXS8047	43.05	−5.63	0.34	0.49	0.51	0.47
DXS1214	46.21	−8.40	−0.66	−0.21	−0.02	0.07
DXS9907	48.55	−8.45	−1.25	−0.75	−0.50	−0.35
DXS8090	56.02	−5.98	0.03	0.20	0.25	0.25
DXS8012	64.51	−5.96	−1.19	−0.65	−0.36	−0.18
DXS1003	72.39	−5.94	−1.18	−0.64	−0.36	−0.18
DXS1204	78.52	−5.61	−0.88	−0.37	−0.12	0.02
DXS8092	86.45	−5.60	−0.65	−0.17	0.06	0.17
DXS990	94.92	−5.59	−0.66	−0.18	0.05	0.17
DXS8096	103.56	−19.43	−2.15	−1.34	−0.89	−0.61
DXS1212	123.88	−10.38	−3.20	−2.10	−1.51	−1.13
DXS8043	160.62	−14.06	−3.46	−2.30	−1.64	−1.18
DXS8103	178.77	−5.96	−1.19	−0.65	−0.36	−0.18

Significant LOD scores are marked with an asterisk. The genetic distances are given according to the Marshfield map.[57]

he had mild peripheral hypotonia, reduced tendon jerks, and mild dysmetria. Renal ultrasounds were normal, and serum transaminases were mildly elevated on at least two occasions. Ophthalmological examination was challenging, and apparent optic nerve atrophy was noted, but no pigment changes were seen.

Linkage Analysis

We performed linkage analysis with 16 markers on the X chromosome (Table 1). A maximum two-point LOD score of 2.07 was obtained for marker DXS8022. It was possible to exclude the remainder of the X chromosome from linkage (LOD score <-2). The interval is delimited by the pseudoautosomal region on the telomeric side and by DXS8036 on the centromeric side (Figure 1A). The 14 Mb interval contains 66 annotated genes (NCBI Map Viewer build 36.3), four of which, *OFD1*, *NLGN4X*, *HCCS*, and *PRPS2*, are included in the ciliary proteome database and thus might encode ciliary proteins.[44] To our knowledge, ciliary localization has only been experimentally proven for the protein encoded by *OFD1*. Mutations in *NLGN4X* are involved in autism and/or mental retardation (MIM 300495), and those in *HCCS* are involved in microphthalmia and linear skin defects (MIM 309801). Mutations in *OFD1* cause OFD1 syndrome and SGBS2. Mutations in *PRPS2* have not been reported.

OFD1 Is Mutated in Joubert Syndrome Patients

Because patients in the families investigated in this report have features in common with OFD1 and SGBS2 patients, we first analyzed *OFD1* in family member III-10. Mutation analysis of all exons and splice sites of *OFD1* showed a deletion of seven base pairs in exon 21: c.2841_2847 delAAAA GAC (p.K948NfsX8) (Figure 1B). The deletion cosegregated with the disease in the family as shown by direct DNA sequencing in all family members and was not present in 190 male controls as shown by ARMS, nor in an additional 250 control chromosomes as shown by direct sequencing (data not shown). Analysis of all *OFD1* exons and splice sites in 65 males with JS and of exons 16–23 in 19 additional male JS patients revealed one de novo mutation, c.2767 delG (p.E923KfsX3), in exon 21 in patient UW87 (Figure 1C). This mutation was not present in 250 control chromosomes as shown by direct sequencing (data not shown) and supports the involvement of *OFD1* in JS. Because *OFD1* escapes X inactivation[45], X inactivation should not be skewed in obligate carrier females. Indeed, in carrier females III-2, III-4, and III-8, there is no preferential expression of either X chromosome (data not shown). The deletion causes a frameshift in the OFD1 protein, resulting in a premature termination codon eight amino acids after I947. This termination codon should, in theory, give rise to nonsense-mediated decay of the *OFD1* mRNA. QPCR analysis of *OFD1* mRNA levels in EBV-LCLs from family member III-9 and isolated patient UW87 showed that 30% and 58%, respectively, of *OFD1* expression remained (Figure S1).

OFD1 Interacts with Lebercilin

OFD1 was identified as an interacting partner of the *LCA5*-encoded protein lebercilin by a GAL4-based yeast two-hybrid screen of a retinal cDNA library; the first 305 N-terminal amino acids of lebercilin were used as a bait. Two independent prey clones that encoded largely overlapping OFD1 fragments, amino acid residues 356–1012 and 240–1012, respectively, were identified. The fragments interacting with lebercilin cover five of the six predicted coiled-coil regions of OFD1 and stretch as far as the C terminus (Figure 3A).[46] Apart from the full-length OFD1 protein of 1012 amino acids ($OFD1^{FL}$), there exists an alternative splice variant that lacks exon 10 and thus encodes a protein ($OFD1^{\Delta ex10}$) lacking the corresponding 40 amino acids encoded by this exon. Both OFD1 splice variants appear to be of similar biological importance because mRNA of both isoforms is equally expressed in several human tissues and protein expression of both isoforms is detected in bovine retinal extracts (Figure S2).

The lebercilin-OFD1 interaction was confirmed in a dedicated yeast two-hybrid assay, in which both OFD1 fragments (amino acid residues 356–1012 and 240–1012) were coexpressed with full-length lebercilin. In order to determine which coiled-coil regions of lebercilin are responsible for OFD1 binding, we coexpressed different combinations of lebercilin deletion constructs fused to GAL4-BD with OFD1 fused to GAL4-AD in yeast, and we assessed protein-protein interactions by monitoring reporter gene activation (Figure 3A). The region containing

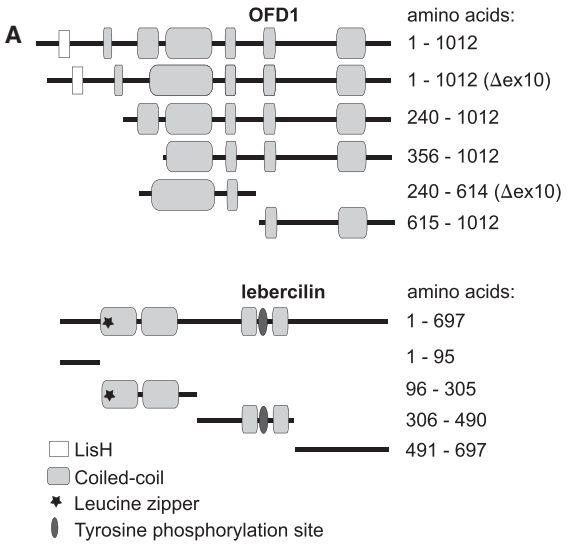

B

AD-OFD1 / BD-lebercilin	aa 240-1012	aa 356-1012	aa 240-614 (Δex10)	aa 615-1012
aa 1-697	+/-	+	++	+/-
aa 1-95	-	-	NA	NA
aa 96-305	++	++	++	+/-
aa 306-490	-	-	NA	NA
aa 491-697	-	-	NA	NA

C

GST	+				
GST-OFD1$^{\Delta ex10}$		+			
GST-OFD1 $^{356-1012}$			+		
GST-OFD1 $^{240-1012}$				+	
GST-nephrocystin-4-I					+
3xFLAG-lebercilin	+	+	+	+	
3xFLAG-RPGRIP1 $^{C2-end}$					+

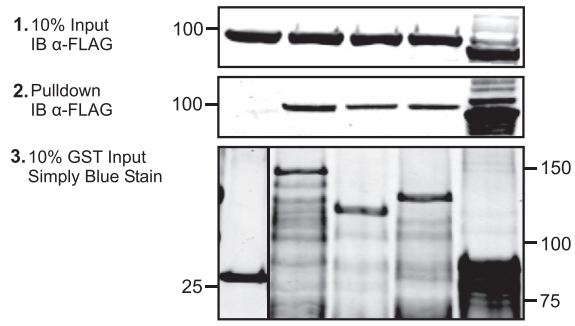

HA-lebercilin	+	+	+	+	+	
HA-nephrocystin-4-I						+
3xFLAG-OFD1 $^{\Delta ex10}$		+				
3xFLAG-OFD1 ^{FL}			+			
3xFLAG-OFD1 $^{356-1012}$				+		
3xFLAG-OFD1 $^{240-1012}$					+	
3xFLAG-LRRK2 ^{LRR}	+					
3xFLAG-RPGRIP1 $^{C2-end}$						+

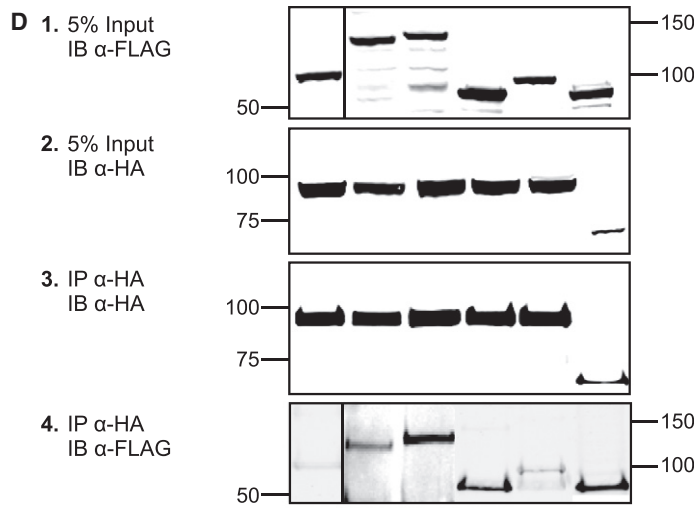

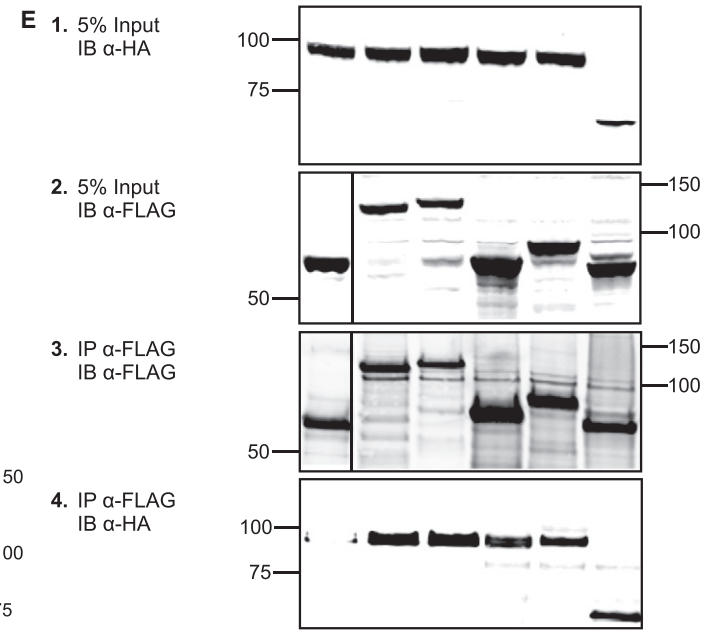

Figure 3. OFD1 Interaction with Lebercilin

(A) OFD1 and lebercilin protein structures. The protein domains of the two OFD1 isoforms (OFD1^{FL} and OFD1$^{\Delta ex10}$) and the OFD1 fragments identified in the yeast two-hybrid screen are depicted, along with the protein domains of the lebercilin fragments expressed by the deletion constructs that were tested for interaction.

(B) Yeast two-hybrid assays confirmed binding of both OFD1 fragments, spanning amino acid residues 240–1012 and 356–1012, to full-length lebercilin and the region containing the first two predicted coiled-coil domains of lebercilin. OFD1 fragments containing coiled-coil domains two/three and four (amino acids 240–614 Δex10 [Δaa313–353]) and coiled-coil domains five and six (amino acids 615–1012) both interacted with full-length lebercilin and with the lebercilin fragment spanning amino acids 96–305, although the OFD1 fragment containing coiled-coil domains two/three and four showed the highest affinity. NA = not analyzed; activation of the *HIS3* and *ADE2* reporter genes is qualitatively indicated by – (no growth on selective media), +/− (slow growth), + (growth), or ++ (fast growth). The activation of the *MEL1* (α-galactosidase activity) and the *LacZ* (β-galactosidase activity) reporter genes was in line with these results.

the first two coiled-coil domains of lebercilin (amino acid residues 96–305, lebercilin^{CC1+2}) was identified as the region with the highest OFD1 binding affinity on the basis of growth on selective media (activation of the *HIS3* and *ADE2* reporters) and both α- and β-galactosidase activity assays (Figure 3B). Similarly, *OFD1* constructs encoding coiled-coil domains two/three and four (amino acid residues 240–614 Δex10 [Δaa313–353]) and coiled-coil domains five and six (amino acid residues 615–1012) were cloned from the OFD1$^{\Delta ex10}$ splice variant and tested in a yeast two-hybrid assay (Figure 3A). Both regions of OFD1 interacted with full-length lebercilin and with amino acid residues 96–305 of lebercilin, but the binding affinity of coiled-coil domains two/three and four was the highest (Figure 3B).

To validate the interaction between OFD1 and lebercilin, we performed both GST pull-down and coimmunoprecipitation assays. For the GST pull-down assay, both OFD1 variants (OFD1^{FL} and OFD1$^{\Delta ex10}$), as well as the OFD1 fragments encompassing amino acids 240–1012 (OFD1$^{aa240–1012}$) and 356–1012 (OFD1$^{aa356–1012}$), were expressed as GST fusion proteins. All of these fragments pulled down 3xFLAG-tagged full-length lebercilin from COS-1 cell lysates (Figure 3C). In a control experiment for specificity, unfused GST failed to pull down lebercilin completely. To assess coimmunoprecipitation of OFD1 with lebercilin, we expressed HA-tagged lebercilin in HEK293T cells together with the previously mentioned OFD1 splice variants and fragments fused to a 3xFLAG-tag. Upon immunoprecipitation of HA-lebercilin via anti-HA beads, all 3xFLAG-OFD1 protein variants and fragments coprecipitated (Figure 3D), although 3xFLAG-OFD1$^{\Delta ex10}$ and 3xFLAG-OFD1$^{aa240–1012}$ apparently coprecipitated less efficiently. The unrelated 3xFLAG-LRRK2 protein did not coprecipitate with HA-lebercilin; this finding confirmed specificity of the interaction between lebercilin and OFD1 in the coimmunoprecipitation assay. (Figure 3D). The coimmunoprecipitation experiment was repeated with anti-FLAG beads in the immunoprecipitation step. Again, coprecipitation of HA-lebercilin with 3xFLAG-OFD1 was observed. In this experimental set up, 3xFLAG-OFD1$^{\Delta ex10}$ and 3xFLAG-OFD1$^{aa240–1012}$ bound more efficiently; therefore, no conclusions on the relative interaction efficiencies of the OFD1 fragments can be drawn. To provide additional evidence for the OFD1-lebercilin interaction, we performed coimmunoprecipitation assays in which the 3xFLAG and HA tags for OFD1 and lebercilin were swapped. These experiments corroborated our previous findings: again, coprecipitation of both proteins could be observed (Figure S3).

Colocalization of OFD1 with Lebercilin

To provide in vivo support for the in vitro OFD1-lebercilin interaction, we performed colocalization experiments in ciliated hTERT-RPE1 cells and rat retina. GFP-OFD1 was previously reported to be targeted to the centrosome because it colocalized with the centrosomal marker γ-tubulin in HEK293 cells.[46] Lebercilin localizes at the basal body and primary cilium, but association with microtubules has been observed as well.[29] We found that upon expression in hTERT-RPE1 cells, eCFP-OFD1^{FL} and eCFP-OFD1$^{\Delta ex10}$ showed a characteristic pericentriolar localization concentrated around the basal body, which was costained with the basal-body and cilium marker α-glutamylated tubulin (GT335) (Figures 4A–4F). A similar localization has also been reported for CEP290 and PCM-1.[47,48] This characteristic localization did not depend on the presence of exon 10 in the *OFD1* construct: both splice variants showed similar pericentriolar localization. When we coexpressed eCFP-OFD1$^{\Delta ex10}$ and mRFP-lebercilin in hTERT-RPE1 cells, partial colocalization was observed (Figures 4G–4I). In rat photoreceptor cells, both OFD1 and lebercilin localize to the connecting cilium region, which is essentially the ciliary transition zone (Figures 4J–4O). This specific connecting cilium localization was evident from costaining of both proteins with the cilium marker centrin.

OFD1 Mutations Reduce Interaction with Lebercilin and Change Ciliary Localization

To explain the phenotypic spectrum observed for *OFD1* mutations, we tested whether six *OFD1* mutations, p.K948fs and p.E923fs (XL-JS; this report), p.I784fs (OFD1[49]), p.E709fs (SGBS2[28]), p.N630fs (OFD1[50]), and p.S586fs (OFD1[27]), affect interaction with lebercilin and/or subcellular localization. In a yeast two-hybrid interaction assay, the p.I784fs, p.N630fs, and p.S586fs mutations completely disrupted interaction of OFD1 with the fragment containing the predicted coiled-coil domains 1 and 2 of lebercilin, as evidenced by the fact that none of the reporter genes for interaction were activated (Figure 5A). For the p.E923fs mutant, yeast growth was significantly reduced in comparison to wild-type OFD1 under conditions selecting for interaction, indicating a reduced binding affinity. The p.K948fs mutation only slightly

(C) Both GST-OFD1 $^{\Delta ex10}$ and the GST-fused OFD1 fragments spanning amino acid residues 240–1012 and 356–1012 (10% input of the assay shown in panel 3) efficiently pulled down 3xFLAG-tagged full-length lebercilin (10% input shown in panel 1; pull-down assay shown in panel 2). Unfused GST failed to pull down lebercilin at all, whereas, in a positive control experiment, GST-nephrocystin-4-I pulled down RPGRIP1^{C2-end}.

(D) The immunoblot (panel 4) shows that 3xFLAG-tagged OFD1 fragments coimmunoprecipitated with HA-lebercilin, whereas the unrelated 3xFLAG-LRRK2 protein did not. Five percent of the cell lysate inputs used in the assays are shown in panels 1 and 2, and the HA immunoprecipitates are shown in panel 3. As a positive control, 3xFLAG-RPGRIP1^{C2-end} coimmunoprecipitated with HA-fused nephrocystin-4-I.

(E) When anti-FLAG immunoprecipitation was performed, HA-lebercilin coimmunoprecipitated with all 3xFLAG-tagged OFD1 fragments, as shown in the immunoblot in panel 4. Panels 1 and 2 show five percent of the cell lysate inputs used in the assays, and panel 3 depicts FLAG immunoprecipitates.

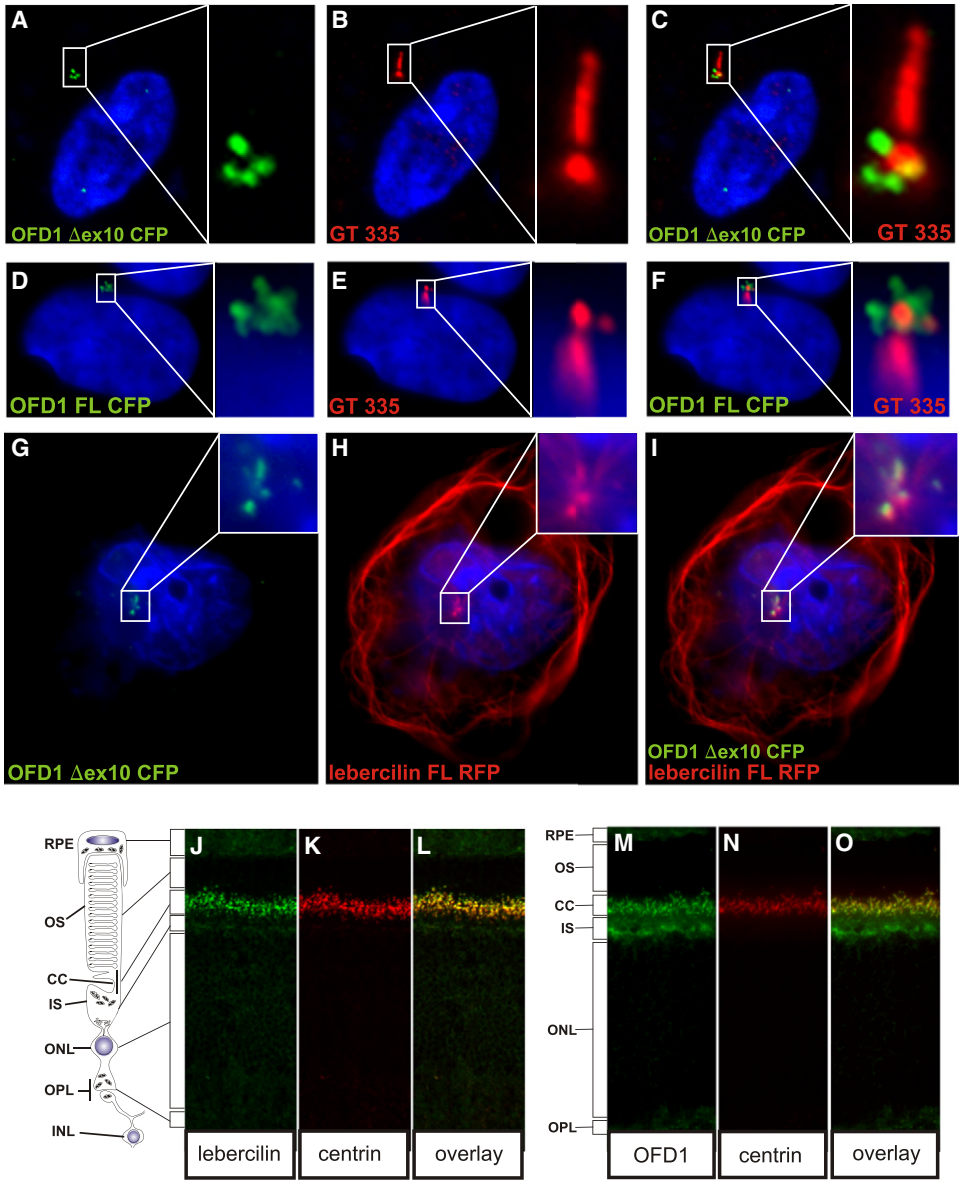

Figure 4. OFD1 and Lebercilin Colocalization in hTERT-RPE1 Cells and Rat Retina

(A–C) Colocalization of eCFP-OFD1$^{\Delta ex10}$ (A, green) and the basal-body and cilium marker GT335 (B, red), a mouse monoclonal antibody against polyglutamylated tubulin. eCFP-OFD1$^{\Delta ex10}$ localizes to the pericentriolar region. (C) is overlay of (A) and (B).

(D–F) eCFP-OFD1^{FL} (D, green) also shows similar pericentriolar localization, as seen from costaining with GT335 (E, red). (F) is an overlay of (D) and (E).

(G–I) Colocalization of eCFP-OFD1$^{\Delta ex10}$ (G, green) and mRFP-lebercilin (H, red). Colocalization is observed at the basal-body region. (I) is an overlay of (G) and (H).

(J–O) Colocalization of lebercilin (J, green) and OFD1 (M, green) with centrin (K and N, red), a marker of the connecting cilium region, in rat photoreceptor cells. (L) and (O) are overlays. In all pictures, nuclei are stained with DAPI (blue). Abbreviations are as follows: RPE, retinal pigment epithelium; OS, outer segment; CC, connecting cilium; IS, inner segment; ONL. outer nuclear layer; OPL, outer plexiform layer; and INL, inner nuclear layer.

reduced yeast growth, whereas the p.E709fs mutation did not apparently affect yeast growth. For the mutants that retained interaction in the yeast two-hybrid assay, we also assessed the effects on lebercilin binding in a semi-quantitative liquid β-galactosidase assay, demonstrating activation of the *LacZ* reporter gene (Figure 5B). This assay showed that the p.E709fs mutation moderately decreased OFD1 binding to lebercilin (60% residual reporter gene activity compared to that of wild-type OFD1). The p.K948fs and p.E923fs mutations more strongly decreased OFD1 binding to lebercilin (24% and 18% residual reporter gene activity, respectively).

We also investigated to what extent *OFD1* mutations influenced cellular localization of the encoded eCFP-fusion protein. In hTERT-RPE1 cells, the JS-associated p.K948fs and p.E923fs mutants (Figures 6A–6F) and the SGBS2-associated p.E709fs mutant (Figures 6J–6L) retained pericentriolar localization, comparable to that of wild-type

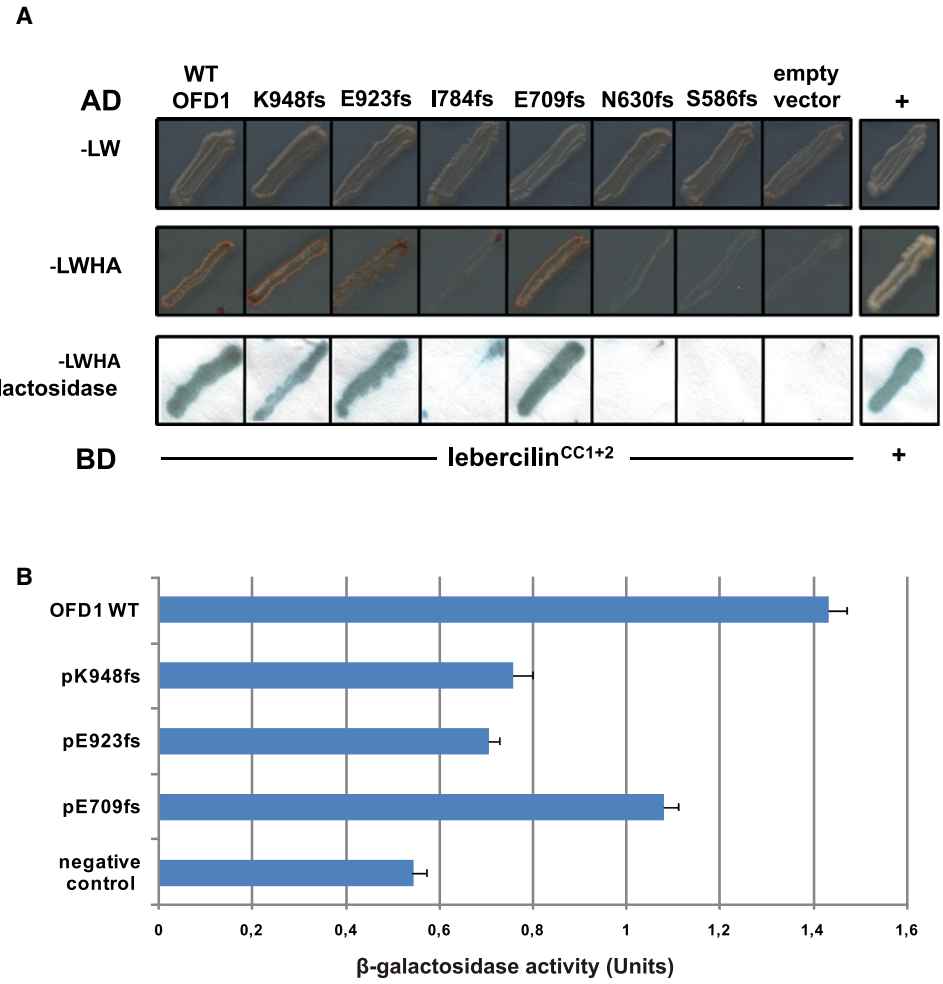

Figure 5. Effect of *OFD1* Mutations on Interaction with Lebercilin

(A) Interaction of wild-type (WT) OFD1 and OFD1 mutants with lebercilin in the yeast two-hybrid assay. Expression constructs encoding the amino acid fragment 356–1012 of OFD1 as GAL4-AD-fusion protein, either wild-type or containing the p.K948fs, p.K923fs, p.I784fs, p.E709fs, p.N630fs, or p.S586fs mutation, were cotransformed with pBD-lebercilin^{CC1+2} constructs in *PJ694α*. As a negative control, the empty pAD vector was cotransformed with pBD-lebercilin^{CC1+2}. Cotransformation of GAL4-AD- and GAL4-BD-expressing plasmids from the Hybrizap kit was used as positive control. Media lacking the amino acids Leu and Trp selected for cotransformants (−LW panel). Additional omission of His and Ade from the media selected for activation of associated *HIS3* and *ADE2* reporter genes (−LWHA panel). Colonies growing under this selection were transferred to a filter for a β-galactosidase assay (−LWHA β-galactosidase panel). Blue staining indicates β-galactosidase activity by activation of the LacZ reporter gene. The interaction of lebercilin^{CC1+2} with wild-type OFD1, as well as with the OFD1 mutants p.K948fs, p.E923fs, and p.E709fs, was detected by growth on −LWHA-selective media and a positive *LacZ* assay. The OFD1 proteins containing the p.I784fs, p.N630fs, and p.S586fs mutations did not interact with lebercilin, as evidenced by the fact that neither growth nor β-galactosidase activity could be detected in the assays.

(B) Liquid β-galactosidase assays revealed that the OFD1 p.K948fs mutation decreased the *LacZ* reporter gene activity to 24% as compared to that of the wild-type (Student t test, p value = 0.0005), indicating a significant reduction in interaction with lebercilin. The p.E923fs mutant retained only 18% of reporter gene activity (p value = 0.0003). For the p.E709fs mutant, 60% of activity remained; this activity level was not significantly different from that of OFD1 wild-type at a p value threshold of 0.005 (p value = 0.03). For the calculation of relative remaining reporter gene activity, values were corrected for background activity in the assay. Error bars represent the standard error of the mean.

eCFP-OFD1. In contrast, the OFD1 syndrome-associated p.N630fs and p.S586fs mutant proteins localized diffusely throughout the cytoplasm and showed only a limited, severely reduced concentration around the basal body (Figures 6M–6R). The p.I784fs mutant protein, which is also associated with OFD1 syndrome, showed comparable scattering throughout the cytoplasm but showed clear concentration at both centrioles (Figures 6G–6I). This localization obviously differed from the pericentriolar localization observed for wild-type OFD1 and for the XL-JS and SGBS2-associated mutant proteins.

Discussion

Until now, Joubert syndrome has been recognized as an autosomal-recessive disorder.[51] In this study, we report that in two unrelated families with X-linked recessive JS

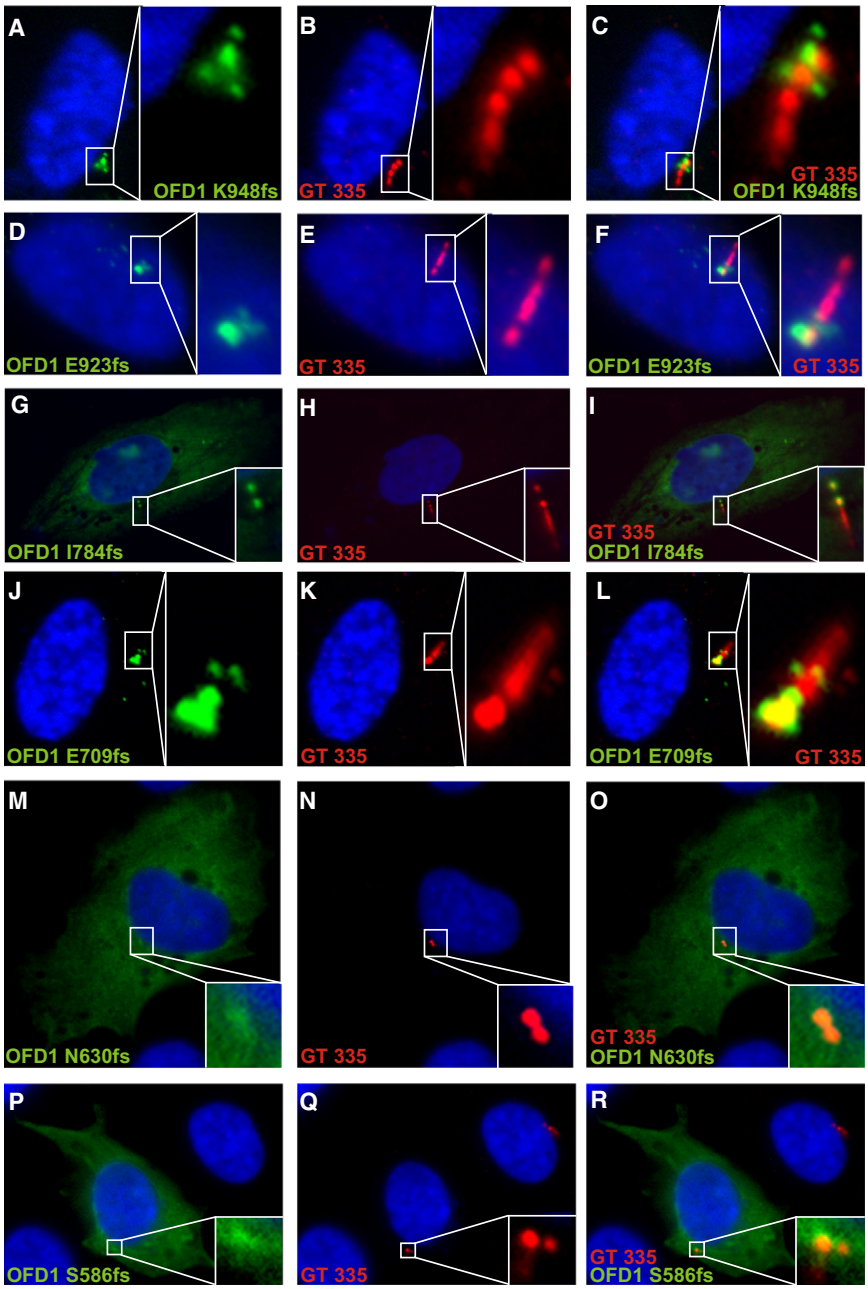

Figure 6. Localization of OFD1 Mutants upon Overexpression in hTERT-RPE1 Cells
(A–C) Colocalization of eCFP-OFD1 p.K948fs (A, green) with the basal body and cilium marker GT335 (B, red). The mutant protein shows pericentriolar localization comparable to that observed for wild-type eCFP-OFD1. (C) is an overlay of (A) and (B).
(D–F) Colocalization of eCFP-OFD1 p.K923fs (D, green) with GT335 (E, red), showing pericentriolar localization. (F) is an overlay of (D) and (E).
(G–I) eCFP-OFD1 p.I784fs (G, green) is scattered throughout the cytoplasm but concentrates at both centrioles, which are indicated by GT335 staining (H, red). (I) is an overlay of (G) and (H).
(J–L) Colocalization of eCFP-OFD1 p.E709fs (J, green) with GT335 (K, red), indicating pericentriolar localization. (L) is an overlay of (J) and (K).
(M–O) eCFP-OFD1 p.N630fs (M, green) localizes diffusely throughout the cytoplasm, and only limited colocalization with GT335 (N, red) is observed. (O) is an overlay of (M) and (N).
(P–R) eCFP-OFD1 p.S586fs (P, green) also shows cytoplasmic distribution and limited colocalization with GT335 (Q, red). (R) is an overlay of (P) and (Q).
In all pictures, nuclei are stained with DAPI (blue).

(as defined by the presence of the molar tooth sign), exon 21 of *OFD1* contains two separate protein-truncating mutations. The mutations cosegregated with the disease and were not found in more than 250 controls. Affected males primarily presented with mental retardation accompanied by postaxial polydactyly. Central apnea was noted in at least one family member of the XL-JS family and in isolated patient UW87. In the XL-JS family, early-onset retinal degeneration was reported, showing that *OFD1* mutations can cause classic JS with retinal involvement.[3] The facial dysmorphism, oral anomalies, and overgrowth in patient UW87 reveal phenotypic overlap between *OFD1*-related JS, SGBS2, and OFD1 syndrome.

The *OFD1* gene has previously been associated with OFD1 syndrome,[27] which is a male-lethal X-linked dominant condition primarily involving malformations of the face, oral cavity, and digits (Table 2). Cystic kidney disease is also commonly associated with this disorder, as are central nervous system abnormalities. However, a molar tooth sign on a brain MRI has never been reported. OFD1 syndrome belongs to the broad spectrum of cilia-related disorders or ciliopathies; the OFD1 protein was found to localize to centrosomes[52] and basal bodies in renal epithelial cells.[46,53] Mice lacking *Ofd1* reproduced the main features of the human disease and showed several hallmarks of ciliary dysfunction, such as failure of left-right axis specification, polydactyly, and renal cyst development.[54] Mutations in *OFD1* have also been found in a single family presenting with X-linked recessive mental retardation, macrocephaly, and respiratory ciliary dyskinesia (SGBS2; Table 2).[28] The index patient in this study, who was the only living affected individual in the family, showed no molar tooth sign on a brain MRI. However, no brain-scan data were available for the other, more severely affected patients, who died soon after birth, so it can not be completely excluded that SGBS2 belongs to the spectrum of JSRDs.

The two XL-JSRD mutations reported here lead to a frameshift that results in a premature termination codon

Table 2. Clinical Features of the XL-JS Family and Isolated JS Patient UW87 as Compared to SGBS2 and Females with OFD1 Syndrome

Clinical Symptom	XL-JS	XL-JS (UW87)	SGBS2[28]	OFD1[58]
General				
Inheritance	recessive	de novo	recessive	dominant
Recurrent infections	+	-	+	-
Juvenile RP	+	-	-	-
Cystic kidneys	-	-	-	+
Obesity	-	+	+	-
Typical age of male death	>20 yrs	>12 yrs	<3yrs	Prenatal
Neurological Findings				
Mental retardation	severe/profound	severe	severe	mild
Hypotonia	-	+	+	-
Central apnea	+	+	-	-
Molar tooth sign	+	+	-	-
Corpus callosum agenesis	-	-	-	+
Dysmorphisms				
Macrocephaly	-	+	+	-
High-arched palate	-	-	+	-
Low-set ears	+	-	+	-
Broad nasal bridge	+	-	-	+
Hypotelorism	-	-	-	+
Hypoplasia of the nasal alae	-	+/−	-	+
Downslanting palpebral fissures	-	-	-	+
Oral Abnormalities				
Cleft lip/palate	-	+/−**	-	+
Tongue abnormalities	-	+	-	+
Abnormal dentition	-	-	-	+
Digital Abnormalities				
(Postaxial) polydactyly	+	+	+	+*
Brachydactyly	-	+	+	+
Clinodactyly	-	-	-	+
Broad thumbs	-	+/−	+	-
Long digits	+	-	-	-

* Postaxial polydactyly has been reported in OFD1 syndrome but occurs rarely (<5%).
** Notched lip.

in the *OFD1* mRNA; this in turn renders the mutant mRNA subject to nonsense-mediated decay. Consequently, only about 30%–60% of *OFD1* transcript persists. This is also the case for the SGBS2 mutation (Figure S1). Most OFD1-syndrome-associated mutations also result in premature termination codons and are thus predicted to reduce transcript levels as well. Therefore, we postulate that the phenotypic variability observed for *OFD1* mutations is primarily caused by changes in activity of the remaining truncated OFD1 protein (Figure 7). Overall, the severity of the phenotype correlates with a reduction in OFD1 protein length. All mutations before amino acid residue 631 are lethal for males and cause OFD1 syndrome in females. The SGBS2-associated p.E709fs mutation causes macroencephaly and early death in males because of severe respiratory-tract infections, but it leaves females unaffected. Male patients with the p.K948fs and p.E923fs mutations, which are located in the coiled-coil domain nearest to the C-terminal end of the protein, have JS and may live beyond the age of 30 years, whereas carrier females

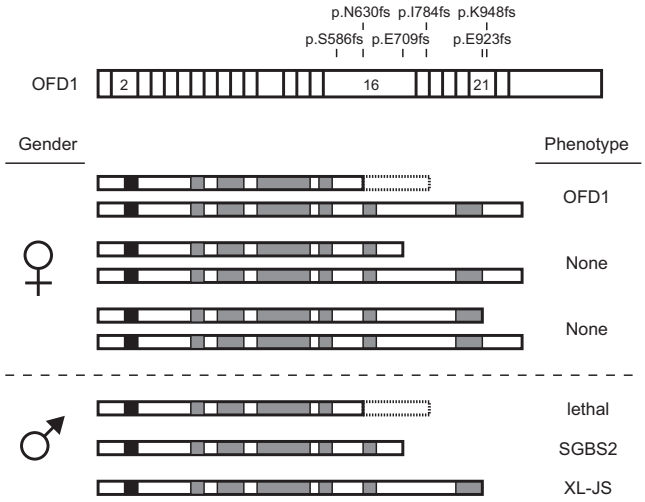

Figure 7. Genotype-Phenotype Correlation of *OFD1* Mutations with OFD1, SGBS2, and XL-JS
Mutations thus far reported as occurring before amino acid residue 631 are all embryonic lethal for males. In females, these cause OFD1 syndrome. The SGBS2-associated p.E709fs mutation causes early death in males, but females are not affected. Male patients with the p.E923fs and p.K948fs mutations that cause XL-JS may live beyond the age of 30 years. We have also indicated the position of the exon 17 p.I784fs mutation that results in OFD1 syndrome in females and is lethal to males to show that the phenotype boundaries are variable (dotted lines). However, the overall severity of the phenotype inversely correlates with the size of the remaining OFD1 protein.

are not affected. Interestingly, two exon 17 mutations that are positioned between the SGBS2 and the XL-JS mutations have been described[49,55]: one is a frameshift (p.I784fs), and one is a deletion of the complete exon. These exon 17 mutations are lethal to males and cause OFD1 syndrome in females. This shows that the phenotypic boundaries are variable and that other factors, such as variable degrees of RNA degradation, contribute to the differences in phenotype as well.

We show that OFD1 physically interacts with lebercilin, the protein encoded by the LCA-associated gene *LCA5*.[29] The functional significance of this interaction is stressed by the fact that the X-linked JS family we report here also suffers from retinal degeneration. For the family members IV-5 and IV-6, as well as for isolated patient UW87, no retinal phenotype could be diagnosed. However, monitoring of these patients is advisable because a retinal pathology could develop in the future. Variability in the onset and severity of the retinal phenotype among and within families is a common feature with isolated RP and even more so in (retinal) ciliopathies, which often express a variable combination of phenotypes.[9] Furthermore, we show that OFD1 is present in retinal photoreceptor cells, where it colocalizes with lebercilin in the transition zone of the photoreceptor sensory cilium. In other cell types, both OFD1 and lebercilin localize to the basal body and/or to primary cilia.[29,46,52] Our interaction data show that the p.K948fs, p.E923fs, and p.E709fs mutations in *OFD1* weakened the interaction with lebercilin but did not totally disrupt it. OFD1-eCFP fusion proteins containing the p.K948fs, p.E923fs, and p.E709fs mutations showed normal pericentriolar localization in hTERT-RPE1 cells. In contrast, the male-lethal dominant OFD1 p.I784fs, p.N630fs, and p.S586fs mutations completely abolished interaction with lebercilin, and upon expression of the corresponding mutated recombinant proteins in hTERT-RPE1 cells, pericentriolar localization was lost completely; however, apart from diffuse cytoplasmic localization, the p.I784fs mutant protein showed concentration at both centrioles, and such an observation was not made for the p.N630fs and p.S586fs mutant proteins. The p.I784fs mutation lies in exon 17, which is further downstream than the p.N630fs and p.S586fs mutations and results in a longer remaining mutant protein. This mutant protein might retain the ability to concentrate at the centrioles, but it has lost pericentriolar localization as well as lebercilin binding affinity. Taken together, these data support the hypothesis that differences in binding affinity of the OFD1 mutant protein to functionally interacting proteins, such as lebercilin, underlie the phenotypic variability observed for OFD1 syndrome, SGBS2, and XL-JS.

The exact cellular function of OFD1 is not known yet, but evidence from studies with knock-out mice shows that OFD1 is required for primary cilia formation and left-right axis specification.[54] In limb buds of these mice, which consistently showed polydactyly, altered expression of *Hoxa* and *Hoxd* genes was observed. These genes regulate limb patterning downstream of Gli3, which is a transcription factor in the Shh pathway.[56] Although Gli3 itself and other players in the Shh pathway showed no altered gene expression in the limb buds of *Ofd1*-null mice, OFD1 disruption could affect Gli3 function, which would explain the upregulation of *Hox* genes. In this line of thinking, it is interesting to note that *Ofd1* knock-out mice show overall phenotypic overlap with *RPGRIP1L*-null mice.[20,26] Studies in *RPGRIP1L*/*Ftm*-null mice identified RPGRIP1L as a necessary component for cilium-mediated Shh signaling.[26] It is tempting to speculate that OFD1 might also be involved in this pathway; such involvement would explain the occurrence of polydactyly in patients with *OFD1* mutations. Furthermore, mutations in the JS gene *Arl13b* were identified as underlying the lethal *hennin* mouse mutant that shows disruption of the ciliary axoneme and displays a Shh-like phenotype, including defective neural-tube patterning and polydactyly.[15] These studies suggest that cilium-mediated regulation of Shh signaling might be a commonly disrupted pathway in JS.

In conclusion, we have identified *OFD1* as a JSRD gene and have expanded the recognized inheritance pattern of JSRDs to include X-linked recessive. Mutations in *OFD1* are now known to be associated with three disorders: OFD1 syndrome, SGBS2, and XL-JS. We propose that the inverse correlation between OFD1 mutant protein length and phenotypic severity could be explained by differences in binding to functionally interacting proteins and disruption of ciliary localization.

Supplemental Data

Supplemental Data include three figures and one table and can be found with this article online at http://www.cell.com/AJHG/.

Acknowledgments

We thank the families for their valuable contribution to this research. We are also indebted to Lydie Burglen (Service de Génétique et Embryologie Médicales CHU Hôpital d'Enfants Armand-Trousseau, Paris, France) for providing the cell lines of the female patient with the p.I271fs mutation and to Saskia van der Velde and Christel Beumer (Department of Human Genetics, Radboud University Nijmegen Medical Centre, Nijmegen, The Netherlands) for expert technical assistance with cell culturing. We thank Ian Glass and Melissa Parisi (Department of Pediatrics, University of Washington School of Medicine and Seattle Children's Hospital, Seattle, USA) for providing clinical details on subject UW87. We also thank Uwe Wolfrum (Johannes-Gutenberg Universität, Mainz, Germany) for providing the hTERT-RPE1 cell line and the α-centrin monoclonal antibody, E. Nigg (Max-Planck Institut für Biochemie, Martinsried, Germany) for providing α-OFD1 serum, Carsten Janke (CNRS Centre de Recherches en Biochimie Macromoléculaire, Montpellier, France) for providing the GT335 monoclonal antibody, and Brunella Franco (TIGEM Telethon Institute of Genetics and Medicine, Naples, Italy) for providing the full-length *OFD1* clone. This work was supported by The Netherlands Organization for Scientific Research (NWO Toptalent-021.001.014 to K.L.M.C. and NWO Vidi-91786396 to R.R.), the Foundation for Retinal Research (R.R. and F.P.M.C.), the Foundation Fighting Blindness (BR-CMM-0808-0451-RAD to R.R.), the United States National Institutes of Health (NCRR 5KL2RR025015 to D.D.), and the March of Dimes Endowment for Healthier Babies (to D.D.).

Received: June 15, 2009
Revised: August 23, 2009
Accepted: September 4, 2009
Published online: October 1, 2009

Web Resources

The URLs for data presented herein are as follows:

Cilia Proteome, http://www.ciliaproteome.org
Human Genome Browser, http://www.genome.ucsc.edu/
Online Mendelian Inheritance in Man (OMIM), http://www.ncbi.nlm.nih.gov/Omim/
Primer3, http://frodo.wi.mit.edu/cgi-bin/primer3/primer3_www.cgi
SMART, http://smart.embl-heidelberg.de/smart/set_mode.cgi?NORMAL=1

References

1. Maria, B.L., Hoang, K.B., Tusa, R.J., Mancuso, A.A., Hamed, L.M., Quisling, R.G., Hove, M.T., Fennell, E.B., Booth-Jones, M., Ringdahl, D.M., et al. (1997). "Joubert syndrome" revisited: Key ocular motor signs with magnetic resonance imaging correlation. J. Child Neurol. *12*, 423–430.
2. Gleeson, J.G., Keeler, L.C., Parisi, M.A., Marsh, S.E., Chance, P.F., Glass, I.A., Graham, J.M., Jr., Maria, B.L., Barkovich, A.J., and Dobyns, W.B. (2004). Molar tooth sign of the midbrain-hindbrain junction: Occurrence in multiple distinct syndromes. Am. J. Med. Genet. A *125A*, 125–134.
3. Valente, E.M., Brancati, F., and Dallapiccola, B. (2008). Genotypes and phenotypes of Joubert syndrome and related disorders. Eur. J. Med. Genet. *51*, 1–23.
4. King, M.D., Dudgeon, J., and Stephenson, J.B. (1984). Joubert's syndrome with retinal dysplasia: neonatal tachypnoea as the clue to a genetic brain-eye malformation. Arch. Dis. Child. *59*, 709–718.
5. Valente, E.M., Salpietro, D.C., Brancati, F., Bertini, E., Galluccio, T., Tortorella, G., Briuglia, S., and Dallapiccola, B. (2003). Description, nomenclature, and mapping of a novel cerebello-renal syndrome with the molar tooth malformation. Am. J. Hum. Genet. *73*, 663–670.
6. Satran, D., Pierpont, M.E., and Dobyns, W.B. (1999). Cerebello-oculo-renal syndromes including Arima, Senior-Loken and COACH syndromes: More than just variants of Joubert syndrome. Am. J. Med. Genet. *86*, 459–469.
7. Verloes, A., and Lambotte, C. (1989). Further delineation of a syndrome of cerebellar vermis hypo/aplasia, oligophrenia, congenital ataxia, coloboma, and hepatic fibrosis. Am. J. Med. Genet. *32*, 227–232.
8. Haug, K., Khan, S., Fuchs, S., and Konig, R. (2000). OFD II, OFD VI, and Joubert syndrome manifestations in 2 sibs. Am. J. Med. Genet. *91*, 135–137.
9. Badano, J.L., Mitsuma, N., Beales, P.L., and Katsanis, N. (2006). The ciliopathies: An emerging class of human genetic disorders. Annu. Rev. Genomics Hum. Genet. *7*, 125–148.
10. Cantagrel, V., Silhavy, J.L., Bielas, S.L., Swistun, D., Marsh, S.E., Bertrand, J.Y., Audollent, S., Attie-Bitach, T., Holden, K.R., Dobyns, W.B., et al. (2008). Mutations in the cilia gene ARL13B lead to the classical form of Joubert syndrome. Am. J. Hum. Genet. *83*, 170–179.
11. Ferland, R.J., Eyaid, W., Collura, R.V., Tully, L.D., Hill, R.S., Al-Nouri, D., Al-Rumayyan, A., Topcu, M., Gascon, G., Bodell, A., et al. (2004). Abnormal cerebellar development and axonal decussation due to mutations in AHI1 in Joubert syndrome. Nat. Genet. *36*, 1008–1013.
12. Eley, L., Gabrielides, C., Adams, M., Johnson, C.A., Hildebrandt, F., and Sayer, J.A. (2008). Jouberin localizes to collecting ducts and interacts with nephrocystin-1. Kidney Int. *74*, 1139–1149.
13. Dixon-Salazar, T., Silhavy, J.L., Marsh, S.E., Louie, C.M., Scott, L.C., Gururaj, A., Al-Gazali, L., Al-Tawari, A.A., Kayserili, H., Sztriha, L., et al. (2004). Mutations in the AHI1 gene, encoding jouberin, cause Joubert syndrome with cortical polymicrogyria. Am. J. Hum. Genet. *75*, 979–987.
14. Sun, Z., Amsterdam, A., Pazour, G.J., Cole, D.G., Miller, M.S., and Hopkins, N. (2004). A genetic screen in zebrafish identifies cilia genes as a principal cause of cystic kidney. Development *131*, 4085–4093.
15. Caspary, T., Larkins, C.E., and Anderson, K.V. (2007). The graded response to Sonic Hedgehog depends on cilia architecture. Dev. Cell *12*, 767–778.
16. Gorden, N.T., Arts, H.H., Parisi, M.A., Coene, K.L., Letteboer, S.J., van Beersum, S.E., Mans, D.A., Hikida, A., Eckert, M., Knutzen, D., et al. (2008). CC2D2A is mutated in Joubert syndrome and interacts with the ciliopathy-associated basal body protein CEP290. Am. J. Hum. Genet. *83*, 559–571.
17. Bielas, S.L., Silhavy, J.L., Brancati, F., Kisseleva, M.V., Al-Gazali, L., Sztriha, L., Bayoumi, R.A., Zaki, M.S., Abdel-Aleem, A., Rosti, R.O., et al. (2009). Mutations in INPP5E, encoding inositol

polyphosphate-5-phosphatase E, link phosphatidyl inositol signaling to the ciliopathies. Nat. Genet. *41*, 1032–1036.
18. Parisi, M.A., Bennett, C.L., Eckert, M.L., Dobyns, W.B., Gleeson, J.G., Shaw, D.W., McDonald, R., Eddy, A., Chance, P.F., and Glass, I.A. (2004). The NPHP1 gene deletion associated with juvenile nephronophthisis is present in a subset of individuals with Joubert syndrome. Am. J. Hum. Genet. *75*, 82–91.
19. Baala, L., Romano, S., Khaddour, R., Saunier, S., Smith, U.M., Audollent, S., Ozilou, C., Faivre, L., Laurent, N., Foliguet, B., et al. (2007). The Meckel-Gruber syndrome gene, MKS3, is mutated in Joubert syndrome. Am. J. Hum. Genet. *80*, 186–194.
20. Delous, M., Baala, L., Salomon, R., Laclef, C., Vierkotten, J., Tory, K., Golzio, C., Lacoste, T., Besse, L., Ozilou, C., et al. (2007). The ciliary gene RPGRIP1L is mutated in cerebello-oculo-renal syndrome (Joubert syndrome type B) and Meckel syndrome. Nat. Genet. *39*, 875–881.
21. Arts, H.H., Doherty, D., van Beersum, S.E., Parisi, M.A., Letteboer, S.J., Gorden, N.T., Peters, T.A., Marker, T., Voesenek, K., Kartono, A., et al. (2007). Mutations in the gene encoding the basal body protein RPGRIP1L, a nephrocystin-4 interactor, cause Joubert syndrome. Nat. Genet. *39*, 882–888.
22. Tallila, J., Jakkula, E., Peltonen, L., Salonen, R., and Kestila, M. (2008). Identification of CC2D2A as a Meckel syndrome gene adds an important piece to the ciliopathy puzzle. Am. J. Hum. Genet. *82*, 1361–1367.
23. den Hollander, A.I., Koenekoop, R.K., Yzer, S., Lopez, I., Arends, M.L., Voesenek, K.E., Zonneveld, M.N., Strom, T.M., Meitinger, T., Brunner, H.G., et al. (2006). Mutations in the CEP290 (NPHP6) gene are a frequent cause of Leber congenital amaurosis. Am. J. Hum. Genet. *79*, 556–561.
24. Helou, J., Otto, E.A., Attanasio, M., Allen, S.J., Parisi, M.A., Glass, I., Utsch, B., Hashmi, S., Fazzi, E., Omran, H., et al. (2007). Mutation analysis of NPHP6/CEP290 in patients with Joubert syndrome and Senior-Loken syndrome. J. Med. Genet. *44*, 657–663.
25. Baala, L., Audollent, S., Martinovic, J., Ozilou, C., Babron, M.C., Sivanandamoorthy, S., Saunier, S., Salomon, R., Gonzales, M., Rattenberry, E., et al. (2007). Pleiotropic effects of CEP290 (NPHP6) mutations extend to Meckel syndrome. Am. J. Hum. Genet. *81*, 170–179.
26. Vierkotten, J., Dildrop, R., Peters, T., Wang, B., and Ruther, U. (2007). Ftm is a novel basal body protein of cilia involved in Shh signalling. Development *134*, 2569–2577.
27. Ferrante, M.I., Giorgio, G., Feather, S.A., Bulfone, A., Wright, V., Ghiani, M., Selicorni, A., Gammaro, L., Scolari, F., Woolf, A.S., et al. (2001). Identification of the gene for oral-facial-digital type I syndrome. Am. J. Hum. Genet. *68*, 569–576.
28. Budny, B., Chen, W., Omran, H., Fliegauf, M., Tzschach, A., Wisniewska, M., Jensen, L.R., Raynaud, M., Shoichet, S.A., Badura, M., et al. (2006). A novel X-linked recessive mental retardation syndrome comprising macrocephaly and ciliary dysfunction is allelic to oral-facial-digital type I syndrome. Hum. Genet. *120*, 171–178.
29. den Hollander, A.I., Koenekoop, R.K., Mohamed, M.D., Arts, H.H., Boldt, K., Towns, K.V., Sedmak, T., Beer, M., Nagel-Wolfrum, K., McKibbin, M., et al. (2007). Mutations in LCA5, encoding the ciliary protein lebercilin, cause Leber congenital amaurosis. Nat. Genet. *39*, 889–895.
30. Nannya, Y., Sanada, M., Nakazaki, K., Hosoya, N., Wang, L., Hangaishi, A., Kurokawa, M., Chiba, S., Bailey, D.K., Kennedy, G.C., et al. (2005). A robust algorithm for copy number detection using high-density oligonucleotide single nucleotide polymorphism genotyping arrays. Cancer Res. *65*, 6071–6079.
31. Miller, S.A., Dykes, D.D., and Polesky, H.F. (1988). A simple salting out procedure for extracting DNA from human nucleated cells. Nucleic Acids Res. *16*, 1215.
32. Rozen, S., and Skaletsky, H. (2000). Primer3 on the WWW for general users and for biologist programmers. Methods Mol. Biol. *132*, 365–386.
33. Oetting, W.S., Lee, H.K., Flanders, D.J., Wiesner, G.L., Sellers, T.A., and King, R.A. (1995). Linkage analysis with multiplexed short tandem repeat polymorphisms using infrared fluorescence and M13 tailed primers. Genomics *30*, 450–458.
34. Brownstein, M.J., Carpten, J.D., and Smith, J.R. (1996). Modulation of non-templated nucleotide addition by Taq DNA polymerase: primer modifications that facilitate genotyping. Biotechniques *20*, 1004–1010.
35. Fishelson, M., and Geiger, D. (2002). Exact genetic linkage computations for general pedigrees. Bioinformatics *18* (*Suppl 1*), S189–S198.
36. Kong, A., and Cox, N.J. (1997). Allele-sharing models: LOD scores and accurate linkage tests. Am. J. Hum. Genet. *61*, 1179–1188.
37. Hoffmann, K., and Lindner, T.H. (2005). easyLINKAGE-Plus–automated linkage analyses using large-scale SNP data. Bioinformatics *21*, 3565–3567.
38. Wall, F.E., Henkel, R.D., Stern, M.P., Jenson, H.B., and Moyer, M.P. (1995). An efficient method for routine Epstein-Barr virus immortalization of human B lymphocytes. In Vitro Cell. Dev. Biol. Anim. *31*, 156–159.
39. de Brouwer, A.P., van Bokhoven, H., and Kremer, H. (2006). Comparison of 12 reference genes for normalization of gene expression levels in Epstein-Barr virus-transformed lymphoblastoid cell lines and fibroblasts. Mol. Diagn. Ther. *10*, 197–204.
40. Livak, K.J., and Schmittgen, T.D. (2001). Analysis of relative gene expression data using real-time quantitative PCR and the 2(-Delta Delta C(T)). Methods *25*, 402–408.
41. Pfaffl, M.W. (2001). A new mathematical model for relative quantification in real-time RT-PCR. Nucleic Acids Res. *29*, e45.
42. Lupas, A., Van, D.M., and Stock, J. (1991). Predicting coiled coils from protein sequences. Science *252*, 1162–1164.
43. Roepman, R., Letteboer, S.J., Arts, H.H., van Beersum, S.E., Lu, X., Krieger, E., Ferreira, P.A., and Cremers, F.P. (2005). Interaction of nephrocystin-4 and RPGRIP1 is disrupted by nephronophthisis or Leber congenital amaurosis-associated mutations. Proc. Natl. Acad. Sci. USA *102*, 18520–18525.
44. Gherman, A., Davis, E.E., and Katsanis, N. (2006). The ciliary proteome database: An integrated community resource for the genetic and functional dissection of cilia. Nat. Genet. *38*, 961–962.
45. Carrel, L., and Willard, H.F. (2005). X-inactivation profile reveals extensive variability in X-linked gene expression in females. Nature *434*, 400–404.
46. Romio, L., Fry, A.M., Winyard, P.J., Malcolm, S., Woolf, A.S., and Feather, S.A. (2004). OFD1 is a centrosomal/basal body protein expressed during mesenchymal-epithelial transition in human nephrogenesis. J. Am. Soc. Nephrol. *15*, 2556–2568.
47. Kim, J., Krishnaswami, S.R., and Gleeson, J.G. (2008). CEP290 interacts with the centriolar satellite component PCM-1 and is required for Rab8 localization to the primary cilium. Hum. Mol. Genet. *17*, 3796–3805.

48. Tsang, W.Y., Bossard, C., Khanna, H., Peranen, J., Swaroop, A., Malhotra, V., and Dynlacht, B.D. (2008). CP110 suppresses primary cilia formation through its interaction with CEP290, a protein deficient in human ciliary disease. Dev. Cell *15*, 187–197.
49. Thauvin-Robinet, C., Cossee, M., Cormier-Daire, V., Van, M.L., Toutain, A., Alembik, Y., Bieth, E., Layet, V., Parent, P., David, A., et al. (2006). Clinical, molecular, and genotype-phenotype correlation studies from 25 cases of oral-facial-digital syndrome type 1: A French and Belgian collaborative study. J. Med. Genet. *43*, 54–61.
50. Rakkolainen, A., la-Mello, S., Kristo, P., Orpana, A., and Jarvela, I. (2002). Four novel mutations in the OFD1 (Cxorf5) gene in Finnish patients with oral-facial-digital syndrome 1. J. Med. Genet. *39*, 292–296.
51. Parisi, M.A., Doherty, D., Chance, P.F., and Glass, I.A. (2007). Joubert syndrome (and related disorders) (OMIM 213300). Eur. J. Hum. Genet. *15*, 511–521.
52. Romio, L., Wright, V., Price, K., Winyard, P.J., Donnai, D., Porteous, M.E., Franco, B., Giorgio, G., Malcolm, S., Woolf, A.S., et al. (2003). OFD1, the gene mutated in oral-facial-digital syndrome type 1, is expressed in the metanephros and in human embryonic renal mesenchymal cells. J. Am. Soc. Nephrol. *14*, 680–689.
53. Giorgio, G., Alfieri, M., Prattichizzo, C., Zullo, A., Cairo, S., and Franco, B. (2007). Functional characterization of the OFD1 protein reveals a nuclear localization and physical interaction with subunits of a chromatin remodeling complex. Mol. Biol. Cell *18*, 4397–4404.
54. Ferrante, M.I., Zullo, A., Barra, A., Bimonte, S., Messaddeq, N., Studer, M., Dolle, P., and Franco, B. (2006). Oral-facial-digital type I protein is required for primary cilia formation and left-right axis specification. Nat. Genet. *38*, 112–117.
55. Thauvin-Robinet, C., Franco, B., Saugier-Veber, P., Aral, B., Gigot, N., Donzel, A., Van, M.L., Bieth, E., Layet, V., Mathieu, M., et al. (2009). Genomic deletions of OFD1 account for 23% of oral-facial-digital type 1 syndrome after negative DNA sequencing. Hum. Mutat. *30*, E320–E329.
56. Spitz, F., Gonzalez, F., and Duboule, D. (2003). A global control region defines a chromosomal regulatory landscape containing the HoxD cluster. Cell *113*, 405–417.
57. Broman, K.W., Murray, J.C., Sheffield, V.C., White, R.L., and Weber, J.L. (1998). Comprehensive human genetic maps: individual and sex-specific variation in recombination. Am. J. Hum. Genet. *63*, 861–869.
58. Gurrieri, F., Franco, B., Toriello, H., and Neri, G. (2007). Oral-facial-digital syndromes: Review and diagnostic guidelines. Am. J. Med. Genet. A *143A*, 3314–3323.